# Corona Ring Improvement to Surface Electric Field Stress Mitigation of 400 kV Composite Insulator

Rabie Salhi, Abdelouahab Mekhaldi, *Senior Member, IEEE,* Madjid Teguar, Omar Kherif, *Member, IEEE,*

***Abstract*— This paper aims to enhance the performance of a 400 kV composite insulator by minimizing electric field stress along its surface using COMSOL Multiphysics. The study employs optimization techniques for the corona ring, initially targeting key parameters such as the ring tube radius, corona ring radius, and corona ring height. Recently used optimization algorithms for engineering applications, namely Constrained Optimization by Linear Approximation (COBYLA), Coordinate Search (CS), and Nelder-Mead (NM), are utilized to determine the most effective one for the optimization purpose. The results indicate that the three algorithms converge around similar values, with COBYLA exhibiting a lower iteration number. Furthermore, our research confirms that increasing the corona tube radius results in a reduction of electric field when considering the other optimized parameters; however, this leads to an increase in the corona ring weight. To resolve this concern, we conduct a re-optimization of the ring shape by targeting eight specific points that form a polynomial interface replacing the original ring. The obtained results demonstrate that the re-optimized shape effectively reduces surface electric field, although it leads to an increase in the ring weight. Nonetheless, this approach aids in identifying critical regions of surface deformation that interact with the electric field. In light of this, we explore an alternative approach that involves replacing the new shape with multiple corona rings positioned in the most deformed regions and then optimizing their positions. This approach helps to achieve better results of surface electric field and overall weight, under clean and polluted surfaces.**

***Index Terms*— composite insulator, COMSOL, optimization, algorithm, corona ring, electric field, re-optimized shape, multiple corona rings.**

## I. Introduction

CONSIDERING the global energy demand, especially for the electrical power, Algeria has aligned itself with the worldwide trend of expanding power generation. The Algerian Electricity and Gas Company, SONELGAZ, is actively engaged in increasing its electric power production capacity, with a particular emphasis on integrating renewable energy sources [1]. This engagement calls for the development and improvement of the power network infrastructure, with a specific focus on enhancing 400 kV lines [2], which play a crucial role in facilitating the energy transition and minimizing energy losses. Notably, insulators hold significant importance within transmission lines, as they serve to withstand both mechanical and electrical stresses [3].

Composite insulators have gained widespread usage in electrical systems [4], mainly due to their numerous advantages, which have contributed to their significant popularity in electrical networks. Notably, these insulators offer several benefits, such as lighter weight, enhanced design flexibility, higher mechanical strength, superior resistance to pollution, and reduced maintenance requirements [5]. Despite their widespread use, these insulators still encounter significant challenges, especially with regards to their polymeric material. An examination of insulator surface materials that have been in service [4] reveals their vulnerability to insulation aging and loss of hydrophobicity caused by natural conditions. Additionally, exposure to surface discharges resulting from electric fields can lead to surface oxidation, negatively impacting insulator performance and reliability.

Addressing these challenges are of the utmost importance to prevent power loss, radio interference, and surface flashovers, which can ultimately result in electrical breakdowns [6]. To this end, researchers in [7] have focused on enhancing the performance of composite insulators by implementing a textured finish on the silicone rubber surface. This technique effectively increases the creepage length and flashover voltage, leading to significant improvements in insulator performance. Despite the complexity of the insulating systems, researchers can study and understand them effectively through simulation techniques. Reducing the electric field at the insulator surface to enhance its performance using simulation, helps to improve insulating performance before implementation, resulting in significant time and resource savings [2]-[6]-[8]-[9].

For instance, in order to mitigate high electric field stress at the insulator surface, particularly in critical regions near the HV and ground sides, researchers have achieved positive results by redesigning the housing material (silicone rubber) adjacent to those regions [10]. Furthermore, the use of a non-linear resistive field grading material (FGM) in proximity to these regions, as explored in [11], has demonstrated a considerable reduction in the surface electric field.

The corona ring is widely used as an alternative solution to reduce the surface electric field. For voltages exceeding 345 kV, it becomes necessary to install the corona ring on

R. Salhi, A. Mekhaldi and M. Teguar are with the Laboratoire de Recherche en Electrotechnique (LRE), Ecole Nationale Polytechnique (ENP), B.P. 182 El Harrach, Algiers 16200, Algeria. e-mail: (rabie.salhi@g.enp.edu.dz).

O. Kherif is with the Advanced High Voltage Engineering Research Centre, School of Engineering, Cardiff University, Cardiff CF24 3AA, UK. e-mail: (kherifo@cardiff.ac.uk).

both the HV and ground sides [3]. However, the geometry design of the corona ring lacks universally fixed standards [5], and there are no established limitations for the electric field at the insulator surface. To address this, the Electric Power Research Institute (EPRI) extensively investigated and recommended a maximum value of 4.2 kV/cm [12] to prevent radio interference, corona discharge, and mitigate polymer degradation, etc. Consequently, numerous researchers [2]-[6]-[13] have conducted studies to determine the optimal corona ring radius and position that effectively reduce high electric field stress at the insulator surface. These studies utilize optimization techniques to achieve improved outcomes.

Various optimization methods have been applied to enhance the corona ring, including the Multi-Objective Ant Lion Optimizer (MOALO) [2], Particle Swarm Optimization (PSO) [5], and Grey Wolf Optimization (GWO), recommended by the authors [13].

In general, increasing the corona ring tube radius at the optimized position can lead to a more uniform distribution of the electric field and a reduction in the intensity of electric field stress [2]. However, practical limitations must be taken into account, as a larger corona ring tube radius may result in increased material requirements, leading to higher costs and potential mechanical constraints [5]. Additionally, a common reference value for the maximum electric field at the surface of the corona ring is 21 kV/cm [14], which is widely considered not to be exceeded. In recent years, various optimization methods, including COBYLA [15], CS, and NM [16], have been employed to overcome engineering problems. For instance, COBYLA was recently introduced to optimize the design and mass of wind turbine blades [15]. An optimization study, employing the CS algorithm among other techniques [17], was conducted on a ground heat pump system to achieve an optimal balance between cost, performance, and system capacity. The NM technique has also been employed to optimize the design of fiber layer schemes for composite pressure vessels [8]. Moreover, researchers in [16] demonstrated the efficiency of CS and NM in optimizing hyper-parameters in deep learning.

This research focuses on improving the performance of a 400 kV insulator by mitigating surface electric field stress. Transmission lines, towers, clamps, and other accessories are not considered in our simulation. The insulator design is simulated using 2D-axisymmetric mode in COMSOL Multiphysics. We employ three recently developed optimization methods for solving multi-engineering tasks: COBYLA, CS, and NM. Firstly, we optimize the ring tube radius, corona ring radius, and corona ring height. Secondly, we utilize the most effective method to re-optimize the corona ring through its shape. While this technique effectively reduces the surface electric field. It also increases the overall weight. Finally, in order to enhance both the electrical and mechanical performance of the insulator, we replace the re-optimized shape with multiple corona rings. The investigation is conducted considering a clean surface state as well as a uniform pollution layer.

## II. Composite Insulator and Corona Ring

The design of the 400 kV composite insulator (Fig. 1(a)) comprises two end-fittings for HV and ground, housing material made of silicone rubber, and a Fiberglass-Reinforced Plastic (FRP) core to enhance mechanical strength. Other components such as towers, lines, and accessories (clamps, etc.) are not considered in our simulation. The insulator is characterized by the following specifications: shed diameters $d1$ and $d2$ of 181 and 95 mm, with a total of 36 and 70 sheds respectively, and a spacing of $d3$ = 78 mm between them [18]. The overall length of the insulator is $L$ = 3200 mm, with a leakage path $Lp$ of 12100 mm.

This study is conducted using COMSOL Multiphysics, a software platform based on FEM, to model the insulator in a 2D-axisymmetric simulation. Although the model is 2D, the results are presented in a true 3D representation. The material parameters are assigned to the model, with the relative permittivity of the silicone rubber, core, air, the metallic parts (end-fittings and corona ring) and the pollution layer being 4.3, 7.2, 1.0005, 1 and 80 respectively. Their electrical conductivities are $10^{-14}$, $10^{-12}$, $10^{-18}$, $10^{4}$ and $6\text{x}10^{-7}$ (S/m) [2]-[11]-[18]. A uniform pollution, saturated with water, is applied with a thickness of 1 mm [11].

The AC/DC electric currents is applied to the insulator. The lower end-fitting is energized with a voltage of $400/\sqrt{3}$ kV (phase-to-ground), while the upper one is grounded (Fig. 1(a)). A finer free triangular mesh is used for the insulator, and a normal mesh is employed for the surrounding air, represented by a circular region with a radius of 5200 mm.

Critical regions, including the insulator surface, inner fiberglass rod, end-fittings, and corona rings, require careful control of the electric field, particularly on the triple point, formed by the end-fitting, polymer, and air [2], to prevent corona discharge, energy losses…etc [6]. For that, a corona ring is suggested at both the HV and ground ends for voltages exceeding 345 kV [3]; there is no universally fixed radius or position as it depends on specific system requirements. In this study, the corona ring is initially placed at $H$ = 200 mm, $R$ = 200 mm, and $r$ = 15 mm, according to the coordinate system presented in Fig. 1(b). A wall thickness of 2 mm is adopted for the corona ring tube, which is a common choice for corona rings made of aluminum alloy (AA) 6063A [19], known for its density of 2.69 g/cm$^3$. The following are the maximum electric field values set as thresholds in all simulations:

- 4.2 kV/cm along the leakage path (insulator surface) [12]
- 21 kV/cm surrounding metallic parts and corona ring surfaces [14]

## III. Optimization Techniques Arrangement

### A. Optimization Methods

Several attempts have been made to optimize the corona ring using various optimization methods, including the Multi-Objective Ant Lion Optimizer (MOALO) [2] and Particle Swarm Optimization (PSO) [5]. In this section, an overview is provided of the optimization methods employed in this study. Generally, the optimization algorithm is designed to determine the optimal combination of horizontal position $(R)$, vertical

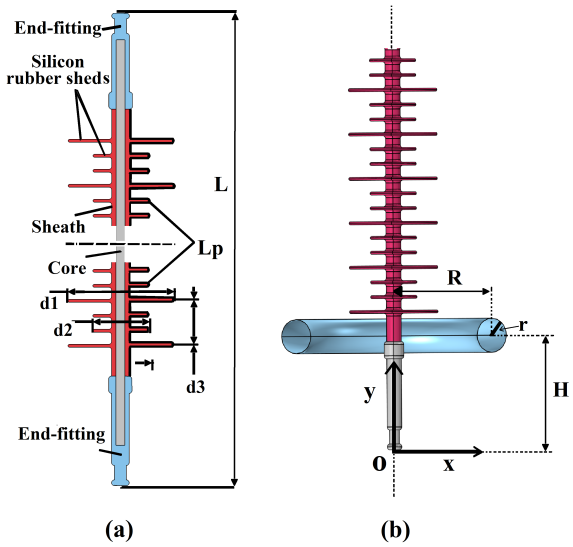


Fig. 1. Insulator design details (a) composite insulator (b) corona ring position on the coordinate system.

position $(H)$, and ring tube radius $(r)$ that results in the lowest electric field while satisfying the specified constraints. The objective is to find a single solution that minimizes the objective function $f(x)$ (maximum electric field along the insulator surface) while adhering to the constraints $g_i(x)$ on the positions and radius, $x$ is a vector of m decision, where:

$$f(x) = max(Electric - field) \tag{1}$$

Subject to:

$$g_i(x) \leq 0, i = 1, 2, \ldots, n. \tag{2}$$

$$x = [x_1, x_2, \ldots, x_m] \tag{3}$$

The COBYLA, CS, and NM methods have gained significant recognition in the field of design optimization [8]-[15]-[17]. Consequently, these methods have been chosen to be utilized in this investigation to identify the effective method for obtaining the optimal solution. Below, a brief explanation of each method is provided:

*1) Constrained Optimization by Linear Approximation (COBYLA):* Constrained Optimization by Linear Approximation COBYLA is a derivative-free optimization algorithm used to solve constrained optimization problems of the objective functions. The algorithm aims to minimize the objective function while satisfying the given constraints. Through iterative adjustments of perturbation size and solution updates, it progresses towards the optimal solution. A comprehensive description of the algorithm can be found in [20] and a brief explanation is given below:

- **Step 1: Initialization**
  Set the maximum number of iterations
  Set the objective function (1) and the constraints (2)
  (The following steps repeated until convergence or reaching the maximum number of iterations)
- **Step 2: Approximation construction**
  Build a linear model $c_i^k(x)$ of the constraint functions (2) to solve the following sub-problem:

$$\min_{x \in \mathbb{R}^n} f^k(x) \tag{4}$$

  Subject to :

$$c_i^k(x) \leq 0 \tag{5}$$

$$||x^k - x|| \leq \Delta^k \tag{6}$$

  Generate a set of points within the trust region $\Delta$ in (6). Starting from zero to $\Delta^k$, to create a linear path from $x^k$ to the solution.
- **Step 3: Update the trust**
  Update the trust region path by adjusting the active sets of the linear constraints (5) based on the agreement between the approximations and the evaluations.
- **Step 4: Convergence check**
  Terminate the algorithm if the improvement in the objective function is achieved and the constraints are satisfied, or when the maximum of iterations is reached.

*2) Coordinate Search (CS):* Coordinate search is an iterative optimization algorithm designed to explore the feasible region of a problem's parameter space to find the optimal solution. The CS algorithm is well-detailed in [16], and a concise description of this algorithm is provided below:

- **Step 1: Initialization**
  Set an initial solution point $x_0$ in the parameter space and a maximum number of iterations.
  Compute the objective function value at the initial solution, $f(x_0)$.
  (The next steps are repeated until convergence or reaching the maximum number of iterations)
- **Step 2: Coordinate iteration**
  Update the coordinate value by searching along the coordinate direction.
  Evaluate the objective function at the updated solution.
- **Step 3: Update step size**
  Update the step size based on the improvement in the objective function, using for example the adaptive step size control or fixed step size reduction.
- **Step 4: Stopping criteria**
  Stop the calculation upon reaching a maximum number of iterations or achieving a desired level of convergence.

*3) Nelder Mead (NM):* The Nelder-Mead method is a derivative-free optimization algorithm that iteratively adjusts a simplex to converge towards the optimum. It employs reflection, expansion, contraction, and shrinkage operations to explore the search space. The algorithm is summarized below, and further details can be found in [21]:

- **Step 1: Initialization**
  Select an initial simplex $Y$ formed by a set of points.

$$Y = [y^0, y^1, \ldots, y^n] \tag{7}$$

  Define a maximum number of iterations.
- **Step 2: Ordering**
  Evaluate the objective function at each point of the simplex (7) and order the points from best to worst based on the function values.

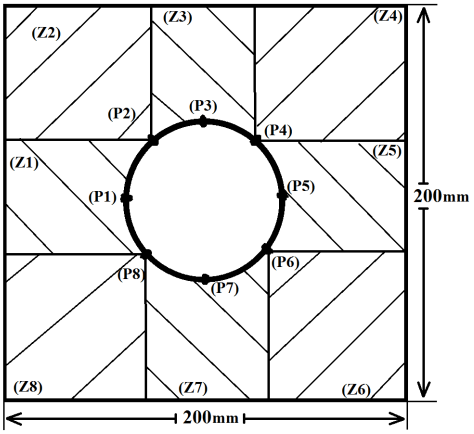


Fig. 2. Free polynomial closed shape with eight points replacing the corona ring in the designated zone.

- **Step 3: Transformation**
  Calculate the new simplex from the current one by replacing the worst vertex with a better point. If the new point is better than the second-worst point but worse than the best point, replace the worst point with the new one. Perform **reflection, expansion, contraction**, or **shrink** operations based on the performance of the new point compared to other points in the simplex.
  Repeat the transformation step until convergence or a termination criterion is met.
- **Step 4: Termination**
  Terminate the algorithm if the improvement in the objective function is achieved and the constraints are satisfied, or if the maximum of iterations is reached.

## B. Optimization Strategy

In this section, the overall optimization strategy employed in this investigation is outlined. The systematic approach involves implementing selected optimization algorithms to achieve the best solution.

Firstly, the optimization algorithms discussed earlier are utilized to determine the effective method for minimizing the electric field at the insulator surface by optimizing the corona ring parameters, namely the ring tube radius $(r)$, corona ring radius $(R)$, and corona ring height $(H)$. These parameters are delimited in specific ranges: 10 mm $< r <$ 30 mm, 150 mm $< R <$ 500 mm, and 150 mm $< H <$ 500 mm. It is important to note that increasing r reduces surface electric field stress when the optimal values of R and H are maintained [2]. However, a larger ring tube radius also adds weight to the insulator, potentially leading to increased costs and mechanical constraints [5]-[22].

Secondly, in order to address the aforementioned limitation, a shape re-optimization technique is employed, to be applied on the corona ring tube. This process focuses on defining eight free points ($P_i$; i = 1, 2, ..., 8) to create a closed polynomial curve. Each point (Pi) is independently positioned within its designated zone $(Z_i)$, enabling the attainment of a custom-shaped corona geometry confined to a 200x200 mm area, as

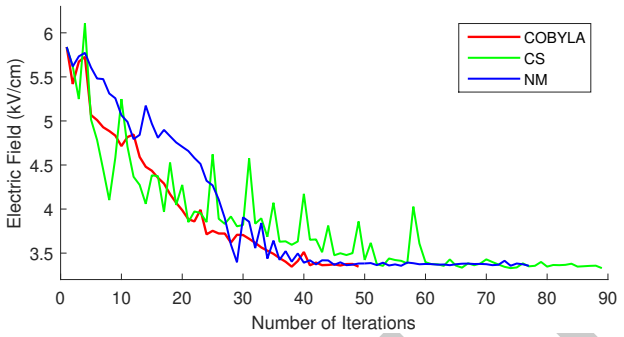


Fig. 3. Convergence of the three-optimization methods used.

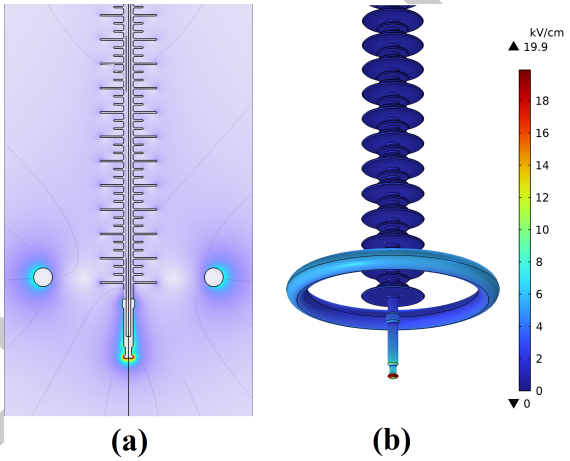


Fig. 4. Electric field distribution for the optimized corona ring under clean surface (a) 2D representation (b) 3D representation.

depicted in Fig. 2. Despite the inevitable enlargement of the corona ring resulting from shape re-optimization (due to the large area that the ring confined in), this approach offers a distinct advantage in identifying critical areas on the ring's surface where deformation occurs. These critical regions are directly associated with the surface electric field stress.

Finally, an alternative approach is put forward to overcome more effectively this limitation. The proposed approach consists of replacing the new shape with multiple corona rings, placed on the critical region. In order to expand the scope of this study, an attempt is made to examine the impact of optimization on weight-optimized structures through a comparative analysis. Their corresponding weights are computed in grams (g) by multiplying their volumes with the density of the aluminum alloy. These volumes are determined directly using the geometric measurement tools available in COMSOL.

TABLE I
OPTIMIZED CORONA RING PARAMETERS FOR THE DIFFERENT OPTIMIZATION METHODS.

| | r(mm) | R(mm) | H(mm) | E-field (V/m) | Iteration number |
|---|---|---|---|---|---|
| COBYLA | 30 | 274.5 | 259.6 | 334630 | 49 |
| CS | 30 | 281.0 | 249.9 | 332980 | 89 |
| NM | 30 | 271.2 | 263.5 | 335630 | 77 |

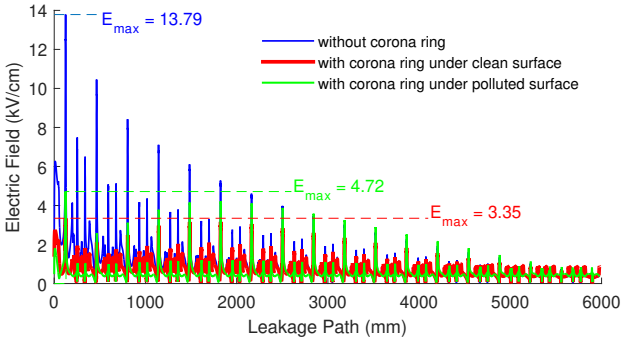


Fig. 5. Electric field distribution along the leakage path with and without the corona ring.

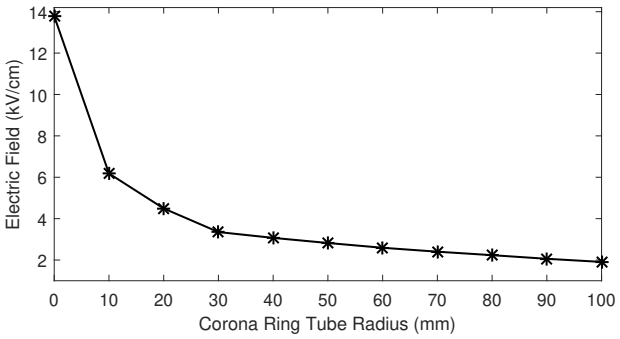


Fig. 6. Variation of maximum electric field along the leakage path for different corona ring radius.

## IV. Findings and Discussion

Taking advantage of the profile symmetry of the insulator along the vertical axis, the investigation was conducted in 2D axisymmetric mode. Both 2D and 3D representations of the electric field distribution across the insulating system (insulator and air surrounding) are provided. To illustrate a clear visualization of the electric field distribution along the leakage path, capitalizing on the symmetry along the horizontal axis (the axis located in the middle of the insulation between the HV and ground ends), all results are presented along half of the leakage path.

The optimization has been applied to the insulator under a clean surface. In regions characterized by intense localized electric fields under pollution condition, significant power dissipation occurs, leading to water evaporation, the formation of dry bands, and the initiation of electrical arcs [11]. Therefore, the effectiveness of the optimization results is subsequently assessed under a uniformly polluted surface.

### A. Optimal Corona Ring Position and Tube Radius Results

By optimizing the corona ring position ($R$ and $H$) and the tube radius ($r$), an optimal configuration can be achieved, effectively reducing the surface electric field stress. As shown in Fig. 3, the solutions obtained by the three methods employed in this study are relatively close, which implies that they converge towards similar points. Notably, the COBYLA method demonstrates rapid convergence compared to the others.

Table I shows the surface electric field values obtained using the three optimization methods, namely COBYLA, CS, and NM, resulting in approximate values of 3.35, 3.33, and 3.37 kV/cm, respectively. The optimized tube radius, $r$, converges to a stable value of 30 mm. In addition, the positioning of the corona ring ($R$ and $H$) demonstrates a balanced configuration around closely-coordinated points. The maximum electric field results consistently remain below the recommended threshold level [12] of 4.2 kV/cm, satisfying essential engineering criteria and effectively mitigating the risk of corona discharge. The COBYLA method exhibits rapid convergence, requiring only 49 iterations to reach the optimal solution compared to the other methods.

The electric field distribution for the optimized corona ring is illustrated in Fig. 4, showcasing both 2D and 3D representations of its intensity. The visualizations reveal higher electric field values in the air surrounding the metallic components, including the corona ring and the energized end (Fig. 4(a)), as well as on their surfaces (Fig. 4(b)). Indeed, it is noteworthy that on the surface of the corona ring, the outer curvature, particularly along the horizontal direction (Ox coordinate), displays the highest level of electric field intensity.

Fig. 5 depicts the distribution of the electric field along the leakage path of the composite insulator, without and with a corona ring for both surface conditions (clean and polluted). As shown in the figure, the electric field distribution at the insulator surface without a corona ring is highly non-uniform, displaying a high intensity near the energized end. However, with the presence of a corona ring under a clean surface, the electric field undergoes systematic adjustment and is redistributed along the leakage path. This results in a more uniform distribution, accompanied by a reduction in the maximum electric field. Without a corona ring, the maximum electric field reaches 13.79 kV/cm. By introducing a corona ring, this electric field is reduced by 75.71 % to attain 3.35 kV/cm. However, in the presence of the corona ring and under the influence of a uniform pollution surface, the maximum electric field increases to reach 4.72 kV/cm.

Indeed, despite achieving surface electric field values below the recommended threshold level with the optimized corona ring under a clean surface, there is a noticeable increase in the surface electric field under a polluted surface, exceeding the recommended threshold level. This necessitates further enhancement of the insulator's performance as much as possible. To achieve this, we conducted additional investigations focusing on increasing the size of the optimized ring while maintaining the same optimized position ($R$ = 271.2 mm, $H$ = 263.5 mm). For this, the tube radius was varied from 10 to 100 mm.

The results obtained are presented in Fig. 6, indicating that the surface electric field decreases as the tube radius ($r$) increases. Expanding the corona ring tube necessitates careful consideration of its associated volume, as it directly affects material requirements, weight, and cost.

### B. Shape Re-optimization Results

The results of reshaping the corona ring surface are attained by simultaneously applying the COBYLA method to eight

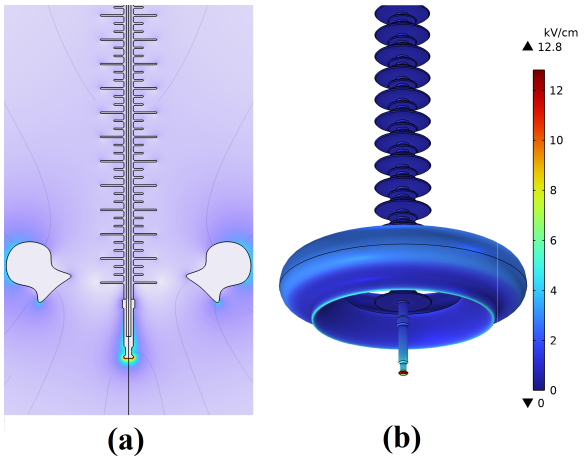


Fig. 7. Electric field distribution for the re-optimized corona ring shape under clean surface (a) 2D representation (b) 3D representation.

points ($P_i$; i = 1, 2, ..., 8). Given the considerable number of points being optimized in this section and to prevent unnecessary lengthening this manuscript, the COBYLA method was chosen. this latter necessitates fewer iterations in contrast to the other techniques employed in this study, while providing favorable results in terms of reducing the electric field along the insulator surface.

The 2D and 3D results of the shape re-optimization are presented in Fig. 7. From this figure, the simulation generates a new form wherein an elongated circular arc is formed in the positive direction between the horizontal and vertical axes. Additionally, two points extend separately towards opposite directions along the horizontal and vertical axes, respectively. In this scenario, heightened electric field intensity is observed in the air surrounding the metallic components, including the re-optimized shape ring and the energized end (Fig. 7(a)), as well as on their surfaces, as shown in Fig. 7(b).

The electric field distribution along the leakage path for optimized corona ring and re-optimized shape ring under both surface conditions (clean and polluted) is illustrated in Fig. 8. Notably, the electric field distribution for the re-optimized shape experiences a substantial reduction compared to the optimized corona ring (Fig. 8(a)). This novel shape leads to a more evenly distributed surface electric field, accompanied by a decrease in the maximum electric field magnitude. The latter is reduced by 50.45 %, achieving a value of 1.66 kV/cm for the re-optimized shape, compared with the 3.35 kV/cm obtained by optimized corona ring.

Considering the re-optimized shape, the maximum electric field under the polluted surface is also reduced (Fig. 8(b)), reaching a value of 2.06 kV/cm compared with the 4.72 kV/cm obtained for the optimized corona ring. This represents a reduction of 56.4 %.

While shape re-optimization effectively reduces the maximum surface electric field, it is worth noting that the optimized points experience significant extension. The new positions of these points, denoted as $P_i$., are presented in TABLE II. This extension inevitably leads to an increase in the volume of the new shape. As a consequence, the measured weight of the

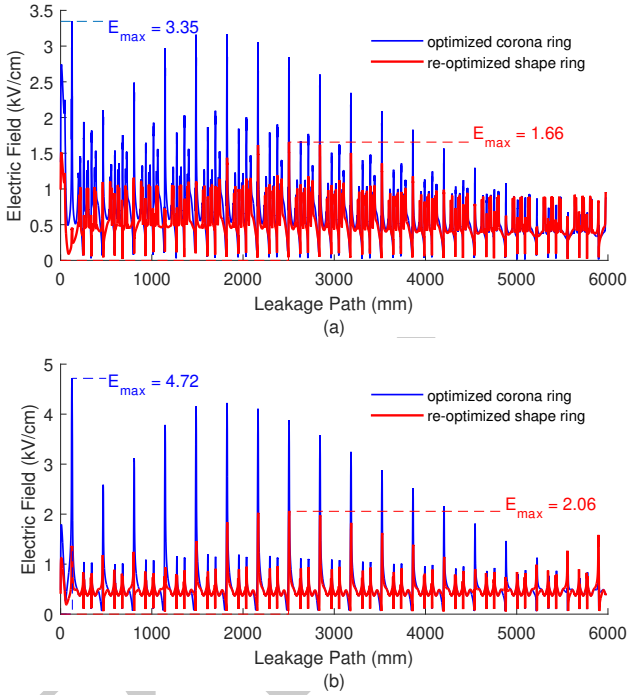


Fig. 8. Electric field distribution along the leakage path for the optimized corona ring and the re-optimized shape ring under (a) clean surface (b) polluted surface.

corona ring is 1680 g, whereas for the re-optimized shape, it reaches 4660 g, representing a weight increase of 177.38 %.

However, the strength of this approach goes beyond the reduction of electric field stress. It also lies in identifying the critical area where the corona tube experiences high deformation, which is closely related to the surface electric field. As a result, the following part discusses how to taking advantage from this findings to simultaneously reduce both the surface electric field and the weight of the corona ring.

### C. Multiple Corona Rings and their Positions Optimization Results

In order to simultaneously minimize the surface electric field and the weight of the corona ring, an investigation is being conducted based on the results derived from the re-optimized shape. It is observed that specific points (P1, P3, P4, P5, and P7) demonstrate significant displacements, as depicted in Fig. 9(a). These points play a crucial role in reshaping the corona ring and achieving the new optimized form, as shown in Fig. 9(b). Accordingly, a strategic decision is made to replace the re-optimized shape with multiple corona rings, effectively addressing concerns related to excessive weight. Consider multiple corona rings, each with a thinner radius

TABLE II
OPTIMIZED POSITIONS OF THE POINTS $P_i$.

| | P1 | P2 | P3 | P4 | P5 | P6 | P7 | P8 |
|---|---|---|---|---|---|---|---|---|
| x(mm) | 185 | 244.5 | 250 | 365 | 370 | 295 | 290 | 229 |
| y(mm) | 265 | 295.5 | 335 | 360 | 245 | 210 | 185 | 230 |

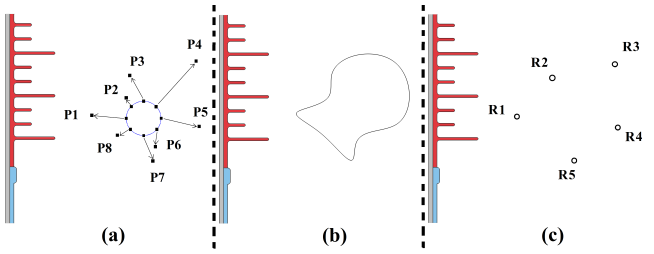


Fig. 9. Re-optimized corona ring shape (a) points displacements (b) new re-optimized shape (c) multiple corona rings.

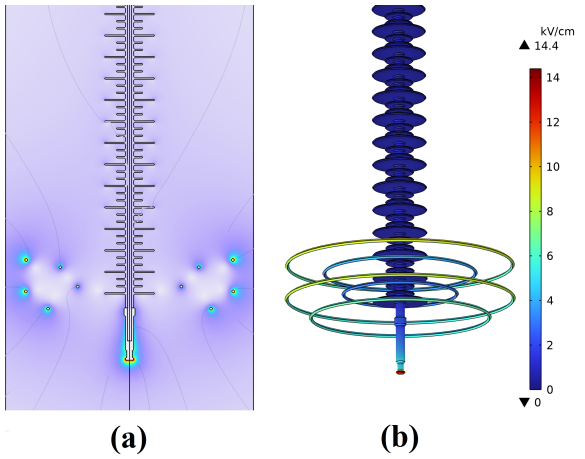


Fig. 10. Electric field distribution for the optimized multiple corona rings under clean surface (a) 2D representation (b) 3D representation.

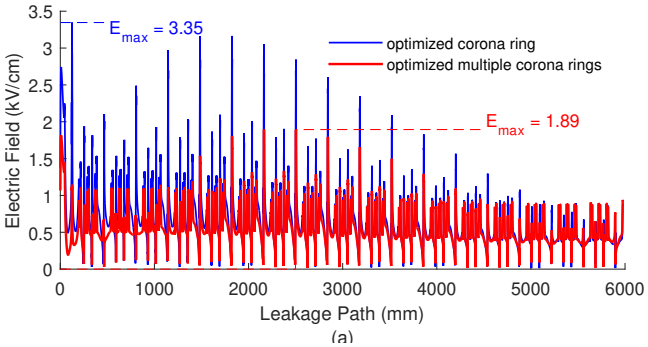


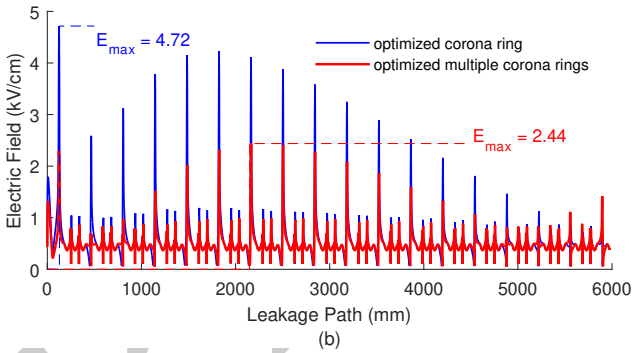


Fig. 11. Electric field distribution along the leakage path for the optimized corona ring and the optimized positions of the multiple corona rings under (a) clean surface (b) polluted surface.

of 5 mm , and their centers are positioned precisely at the coordinates of the aforementioned points (Fig. 9(c).)

The introduction of multiple corona rings resulted in a maximum surface electric field of a 2.10 kV/cm, marking a notable reduction of 37.31 % compared to the optimized corona ring. To further enhance this achievement, an optimization process is performed to reposition the five rings. This process aimed to relocate the center of each ring within a square region defined by a side length of 20 mm (to prevent excessive spacing between the rings). This process contributed to more reduction in the surface electric field to reach a value of 1.89 kV/cm. The new coordinates (in mm) for the center of the multiple corona rings are: R1 (188.3;267.3), R2 (251.5;337.4), R3 (375.1;363.7), R4 (376.6;249.7) and R5 (296;187.3).

Higher electric field intensities are observed in the air surrounding the metallic components, encompassing all the multiple corona rings and the energized end (Fig. 10(a)), as well as on their surfaces, as illustrated in Fig. 10(b).

Fig. 11 illustrates the distribution of the electric field along the leakage path for both optimized corona ring and configuration with multiple corona rings under clean and polluted insulator surface conditions. As shown in the figure, the electric field distribution along the leakage path for the optimized positions of the multiple corona rings exhibits a considerable reduction with regard to the results obtained for the optimized corona ring (Fig. 11(a)). Notably, the surface electric field distribution for the multiple corona rings appears more uniform. Furthermore, a notable reduction in the maximum electric field is observed, with a rate of 43.58 %, where a maximum value of 1.89 kV/cm has been obtained. Considering the same optimized multiple corona rings, under a polluted surface, the maximum electric field is also reduced (Fig. 11(b)), reaching a value of 2.44 kV/cm compared with the 4.72 kV/cm obtained for the optimized corona ring, resulting in a 48.29 % reduction.

Moreover, it is mandatory to ensure that the electric field remains within acceptable limits across all parts of the insulator, particularly for the novel configuration with multiple corona rings. The limit value commonly used is 21 kV/cm. This latter is employed as a reference for the surfaces of corona rings and end-fittings [14] to prevent corona discharge and minimize radio interference, etc. Notably, the highest electric field magnitude surrounding the multiple corona rings for the clean insulator surface is 9.65 kV/cm. It is observed at the surface of the ring (R3). This value is significantly below the limit value, which should not be exceeded.

The technique involves replacing the deformed area of the re-optimized shape with multiple corona rings, aids in decreasing not only the surface electric field but also the weight of the ring. In fact, the measured weight amounts to 1250 g, resulting in a reduction of the corona ring weight by 25.59 %.

## V. Conclusion

This study was conducted to improve the performance of the 400 kV composite insulator by mitigating its surface electric field stress. The investigation focused on optimizing the corona ring radius (R), height (H), and the tube radius

(r). Upon comparing the results derived from the COBYLA, CS, and NM methods, it was observed that such techniques converged toward similar solutions; the COBYLA exhibits rapid convergence.

The optimization resulted in a notable decrease in the maximum electric field along the insulator surface, achieving a value of 3.35 kV/cm. This represents a remarkable reduction of 75.71 % compared to the case without the corona ring. Additionally, it was observed that increasing the tube radius $(r)$ corresponded to a decrease in the surface electric field. However, this accompanied by an increase in the corona ring's volume, leading to excessive weight. To address this issue, the re-optimization of the corona ring's shape approach was explored. As a result, a maximum surface electric field value of 1.66 kV/cm was achieved, marking a reduction of 50.45 % compared to the optimized corona ring. Nevertheless, this technique was associated with an increase in the corona ring's weight by 177.38 %.

Although this weight increase, this re-optimization successfully highlighted critical areas prone to deformations on the corona ring surface. Indeed, the points with significant displacements were replaced by five corona rings, each with a thinner radius, and their positions were optimized. As a result, a significant reduction in the maximum electric field reaching 1.89 kV/cm corresponding to a diminution ratio of 43.58 % with regard to that obtained for optimized corona ring. Moreover, the weight of the corona ring experienced a reduction of 25.59 %. Notably, all electric field values obtained in this investigation are below to the recommended threshold level established by EPRI. In addition, the maximum electric field at metallic parts for the clean insulator was observed at the ring (R3) with a value of 9.65 kV/cm. This latter is much lower than the corona discharge value of 21 kV/cm. The performance under both the re-optimized shape and the multiple corona rings was assessed for uniform pollution condition, revealing a reduction in the maximum electric field by 56.4 % and 48.29 %, respectively, compared to that obtained for the optimized corona ring.

## References


[1] S. Bouacha, A. Malek, O. Benkraouda, A. Hadj Arab, A. Razagui, S. Boulahchiche and S. Semaoui, "Performance analysis of the first photovoltaic grid-connected system in Algeria," *Energy for Sustainable Development,* Vol. 57, pp. 1-11, August 2020, doi: 10.1016/j.esd.2020.04.002.

[2] B. M'Hamdi, Y. Benmahamed, M. Teguar, I. B. M. Taha and S. S. M. Ghoneim, "Multi-objective optimization of 400 kv composite insulator corona ring design," *in IEEE Access,* vol. 10, pp. 27579-27590, 2022, doi: 10.1109/ACCESS.2022.3157384.

[3] "IEEE guide for application of composite insulators," *in IEEE Std 987-2001 (Revision of IEEE Std 987-1985),* pp.1-24, 6 May 2002, doi: 10.1109/IEEESTD.2002.93576.

[4] R. A. Ghunem, L. -L. Tay, H. Terrab and A. H. El-Hag, "Analysis of service-aged 200 kV and 400 kV silicone rubber insulation in the Gulf region," *in IEEE Transactions on Dielectrics and Electrical Insulation,* vol. 23, no. 6, pp. 3539-3546, Dec. 2016, doi: 10.1109/TDEI.2016.006105.

[5] J. A. Diaz-Acevedo, A. Escobar and L. F. Grisales-Noreña, "Optimization of corona ring for 230 kV polymeric insulator based on finite element method and PSO algorithm," *Electric Power Systems Research,* vol. 201, 2021, art. no. 107521, doi:10.1016/j.epsr.2021.107521.

[6] H. Terrab and A. Kara, "Parameters design optimization of 230kV corona ring based on electric field analysis and response surface methodology," *Electric Power Systems Research,* vol. 163, Part B, pp. 782-788, October 2018, doi: 10.1016/j.epsr.2017.06.002.

[7] M. Albano, P. Charalampidis, R. T. Waters, H. Griffiths and A. Haddad, "Silicone rubber insulators for polluted environments part 2: textured insulators," *in IEEE Transactions on Dielectrics and Electrical Insulation,* vol. 21, no. 2, pp. 749-757, April 2014, doi: 10.1109/TDEI.2013.004016.

[8] B. Dai, M. Zhou, J. Zhang, Y. Li, and W. Jin, "Optimization design of filament wound composite pressure vessel based on opensees," *Applied Sciences,* vol. 13, no. 8, April 2023, Art. no. 4894, doi: 10.3390/app13084894.

[9] R. Salhi, A. Mekhaldi, M. Teguar, O. Kherif and M. El Amine Slama, "Cap-pin glass insulator simulation and leakage current waveform extraction," *2022 2nd International Conference on Advanced Electrical Engineering (ICAEE),* Constantine, Algeria, 2022, pp. 1-4, doi: 10.1109/ICAEE53772.2022.9961979.

[10] D. Cruz Dominguez, F. P. Espino-Cortes and P. Gomez, "Optimized design of electric field grading systems in 115 kV non-ceramic insulators," *in IEEE Transactions on Dielectrics and Electrical Insulation,* vol. 20, no. 1, pp. 63-70, February 2013, doi: 10.1109/TDEI.2013.6451342.

[11] M. -R. Halloum, B. S. Reddy and G. N. Reddy, "Stress control for polymeric outdoor insulators using nonlinear resistive field grading materials operating under different conditions," *in IEEE Transactions on Dielectrics and Electrical Insulation* vol. 29, no. 3, pp. 1175-1182, June 2022, doi: 10.1109/TDEI.2022.3164857.

[12] A. J. Phillips, A. J. Maxwell, C. S. Engelbrecht and I. Gutman, "Electric-field limits for the design of grading rings for composite line insulators," *in IEEE Transactions on Power Delivery,* vol. 30, no. 3, pp. 1110-1118, June 2015, doi: 10.1109/TPWRD.2014.2362074.

[13] K. Aramugam, H. A. Illias, Y. C. Ching, M. S. Ali, and M. Z. H. Makmud, "Optimal design of corona ring for 132 kv insulator at high voltage transmission lines based on optimisation techniques," *Energies,* vol. 16, no. 2, Jan 2023, Art. no. 778, doi: 10.3390/en16020778.

[14] A. J. Phillips, J. Kuffel, A. Baker, J. Burnham, A. Carreira, E. Cherney, W. Chisholm, M. Farzaneh, R. Gemignani, A. Gillespie, T. Grisham, R. Hill, T. Saha, B. Vancia, and J. Yu, "Electric fields on ac composite transmission line insulators," *in IEEE Transactions on Power Delivery,* vol. 23, no. 2, pp. 823-830, April 2008, doi: 10.1109/TPWRD.2007.911127.

[15] Z. Zhang, C. Zhang, Y. Qiao, Y. Zhou, and S. Wang, "Design and mass optimization of numerical models for composite wind turbine blades," *Journal of Marine Science and Engineering* vol. 11, no. 1, Jan. 2023, Art. no. 75, doi: 10.3390/jmse11010075.

[16] Y. Ozaki, M. Yano and M. Onishi, "Effective hyperparameter optimization using Nelder-Mead method in deep learning," *IPSJ T Comput Vis,* vol. 9, no. 1, Dec 2017, Art. no. 20, doi: 10.1186/s41074-017-0030-7

[17] H. Moon, H. Kim, and Y. Nam, "Study on the optimum design of a ground heat pump system using optimization algorithms," *Energies,* vol. 12, no. 21, Oct. 2019, Art. no. 4033, doi: 10.3390/en12214033.

[18] M. Bouhaouche, A. Mekhaldi and M. Teguar, "Improvement of electric field distribution by integrating composite insulators in a 400 kV AC double circuit line in Algeria," *in IEEE Transactions on Dielectrics and Electrical Insulation,* vol. 24, no. 6, pp. 3549-3558, Dec. 2017, doi: 10.1109/TDEI.2017.006011.

[19] E. R. Luz, E. L. Romão, S. C. Streitenberger, L. R. Mancilha, A. P. Paiva and P. P. Balestrassi, "A multiobjective optimization of the welding process in aluminum alloy (AA) 6063 T4 tubes used in corona rings through normal boundary intersection and multivariate techniques," *Int J Adv Manuf Technol,* vol. 117, pp. 1517–1534, 2021, doi: 10.21203/rs.3.rs-531184/v1.

[20] T. M. Ragonneau, "Model-based derivative-free optimization methods and software," PhD thesis, Department of Applied Mathematics, The Hong Kong Polytechnic University, 2022.

[21] S. Takenaga, Y. Ozaki, and M. Onishi, "Practical initialization of the Nelder–Mead method for computationally expensive optimization problems," *Optim Lett,* vol. 17, pp. 283–297, 2023. doi: 10.1007/s11590-022-01953-y.

[22] A. Al-Gheilani, W. Rowe, Y. Li and K. L. Wong, "Stress control methods on a high voltage insulator: a review," *Energy Procedia,* vol. 110, pp. 95-100, 2017, doi: 10.1016/j.egypro.2017.03.112.